Solar Powered Switched Reluctance Motor Driven Water Pumping System with Battery Support

Anjanee Kumar Mishra[1*] and Bhim Singh[2], *Fellow, IET*

[1,] Department of Electrical and Computer Engineering, University of Michigan, Dearborn, MI, 48128, USA

*anjaneem@umich.edu

Funding:

This work is finically sponsored by the Department of Science and Technology (DST), Govt. of India, under a project under Grant Number: RP02979 (Indo-UK RESCUES Project) and in part by J-C-Bose Fellowship (Grant Number RP03128) and Fund for Improvement of Science and Technology (FIST, Grant Number RP03195G).

Conflict of interest:

None of the co-authors have a conflict of interest to disclose.

Permission statement to reproduce the materials from the other sources.

"None"

Data Availability Statement:

Data sharing is not applicable to this article as no new data were created or analyzed in this study.

***Abstract*— This work deals with the development of an efficient and reliable solar photovoltaic (PV) fed water pump with a battery energy storage (BES). This system ensures a continuous and rated supply of water in all working conditions. A new control logic for BES is developed, which significantly improves the overall response of the system. The support of the battery as a back-up source is obtained through a bidirectional DC-DC converter. Both the charging/discharging control and maximum power tracking of the solar panel are achieved through this bidirectional converter. Whereas the voltage asymmetry compensation across split capacitors at DC link and motor drive controls are supervised by switched reluctance motor (SRM) converter. The performance of the present scheme is examined through both simulated and experimental responses and found adequate under all operational scenarios.**

Introduction

Among the recent renewable power sources, PV array power is often a best source and available in an endless sum [1]. The primary advantages of solar dependent power stage incorporate clean, contamination-free, brief time establishment, and long-life operation. Some of the limitations

of basics of solar system like its expensiveness, lower conversion ratio, and intermittency in solar power have been successfully overcome in recent times through advancements in solar technologies [2-3].

Therefore, solar-powered water pumps are the most efficient way to utilize the available abundant solar power [4-5]. Innumerable research has been carried out to develop an efficient solar-powered water pumping system (SPWPS) using various electric motor drives [4-7]. Due to the critical nature of water pumping application, there exists a need to utilize a robust, highly reliable, cost-effective, high starting torque and efficient motor drive. Since, the SRM drive has all these required characteristics and, therefore, it is emerging as one of the prominent drives for WPS [8-10].

Nevertheless, various positive aspects of solar-powered systems are there, however, the one major drawback of it is the intermittency in its power [11]. On the other side, the uncertainty in grid power supply, especially in remote and distant areas is still the major constraint with the grid integrated solar water pump [12]. Besides, the voltage fluctuations in the grid voltage in such areas can also damage the system and reduce the overall system reliability. These shortcomings with standalone and grid integrated systems are needed to be considered in order to ensure a reliable and uninterruptable water supply with the efficient operation of the water pumping system [13-14]. Therefore, the standalone system with battery support is one of the unique solutions and is developed in this work. Again, no such system with any of the motor drives including SRM is reported as of now. In addition, the battery connected to the system also provides the constant voltage at the DC link irrespective of any voltage fluctuation in the system.

Therefore, this work is aimed to develop a solar-powered water pumping system, which is reliable and perfect for critical applications like water supply in hospitals, schools, industries, etc. The battery integrated system has served many purposes like storing the solar power in inadequacy, suppressing or smoothing out transients occured in the system due to PV array power supply, and to provide the high magnitude of starting currents to the drive under low insolation levels.

Various attempts are made to develop an SRM driven solar water pump [8-10], [15-16] in which, very few have the storage arrangement [10], [15-16]. One such configuration is reported in [10], which has incorporated the three-phase configuration of SRM. Although, the system has the capacity to offer uninterrupted pumping regardless of the environmental situations, the high-frequency switching signals utilized to operate the motor converter and its of

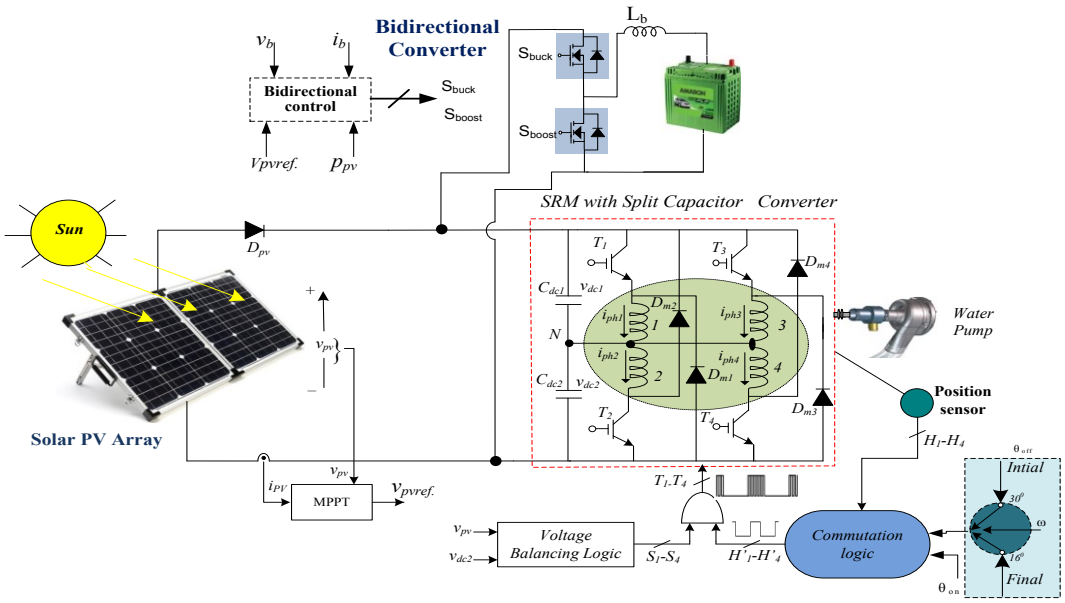

Fig.1 Circuit diagram of present SRM driven solar water pump.

overvoltage limitation under damper failure, result in the configuration less efficient. Besides, the constant-voltage tracing (CVT) technique used for solar power optimization is less effective and faces major limitations under continuously changing environmental conditions. Simulated results showing the battery current has a high value of ripples, which could shrink the performance of the battery. Besides, the execution of an unregulated charging/discharging control approach severely affects the working life span of the battery pack and due to the frequent maintenance required for the system. Another arrangement using an 8/6 pole configuration of SRM drive for solar water pumping is given in [15]. This arrangement is a two-stage system and, therefore the losses are high due to two-stage conversion of solar power before supplied to the drive. Besides, the high ripples in the battery current due to the boost converter diminish the system performance. An isolated control system without incorporating the knowledge variation in solar power badly affects battery performance and its service life. One similar configuration to the present system is discussed in [16] where the MPPT converter is successfully eliminated. However, the developed controller for the scheme has not been tested for all possible mode's operation. Since, the PV power optimization is achieved through the motor control and, therefore, there is no such MPPT control is present when solar PV array is used to charge the battery and pumping is not required. Besides, the uncontrolled charging/discharging of the battery is also one of the major limitations of suggested system.

Thus, the present work has taken care of all the deficiencies present in the aforesaid literature and successfully has overcome them. The bidirectional converter offers both solar power optimization and the charging/discharging control of BES. The PV power is optimized in all possible modes of operation and the elimination of solar output capacitor and DC link voltage sensor, has significantly reduced the overall system cost. The initial winding current suppression at the drive side is also offered in a present system based on the inertia of the motor. The implemented battery management system has significantly improved the system's dynamic performance, especially under

insolation change without using any extra sensors. The major contributions of this work and salient features are as follows.

- An efficient arrangement of a solar power energized water pump with a battery storage scheme is presented in this work.
- The charging/discharging control of the battery is integrated with a bidirectional DC-DC converter. While the optimization of PV array power is achieved using a P&O MPPT control executed through the same bidirectional DC-DC converter.
- Due to the highly inductive nature of motor windings, SRM is the most suitable drive for such configurations.
- A modified version of the P&O MPPT approach is utilized to optimized solar power under all weather conditions.

1. *Configuration of System*

The configuration of the developed system is shown in Fig. 1. The intermediate maximum power tracking converter, which is usually required for MPPT operation is eliminated in this scheme. The PV array power optimization and the battery system control are achieved through the bidirectional converter. Whereas the voltage balancing across split DC link capacitors and motor drive controls are supervised by a mid-point converter. Along with the elimination of the intermediate MPPT converter, this configuration needs the knowledge of voltage across only one split DC link capacitor and the voltage across the other is computed with the help of PV array voltage. Therefore, there is also a reduction in the number of one voltage sensor in comparison to the double-stage configuration.

2. *System Operation*

The developed system has basically four operating modes. The symbolic power flow mechanism for the present system is illuminated in Fig. 2. The battery can directly be connected to the system without any converter. However, the required size of the battery bank is larger in this case, which directly affects the cost and size of the developed system. Moreover, the DC link voltage ripple is to be absorbed by the battery-bank, decreasing its lifetime. One potential way is to rule out these limitations by utilizing a bidirectional DC-DC converter with a battery bank to interface a standalone solar system as shown in Fig.2. Hence, there is wide scope in the selection of the battery terminal voltage magnitude, offering minimization in battery price and its dimension. The bidirectional converter operates as a conventional boost converter to supply the power from the battery to the motor if the PV array power is not able to meet the requirement.

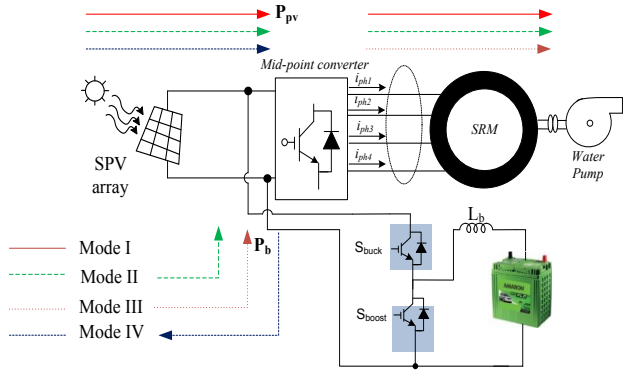

Fig. 2 Schematic of the power flow diagram within the system.

Mode I: Throughout this mode, the solar power generation is adequate to run the pump at its full capacity. So, the battery is neither supply or store the energy and just helps to track the maximum power and maintaining the reference DC link voltage, which is v_{pvref} in the present configuration.

Mode II: In this working scenario, the power coming from the solar panel is inadequate to operate the system alone at rated speed, and therefore, the rest of the power is coming from the battery bank through a bidirectional converter. The bidirectional converter in this mode, acts as a boost converter. The IGBT switch S_{boost} of the bidirectional converter is operated while the reverse diode of switch S_{buck} provides the path for the remaining part of the current flow.

Mode III: This is the situation when there is no solar power generation. In this case, the total required power is coming through BES. The bidirectional converter has yet again functioned in the boost mode with a duty cycle of D_{b1}=0.77. The operation is like mode II, however, with a higher battery current and power.

Mode IV: It is the condition when the solar power is coming into the system and water is not required. Thus, available PV array power is utilized to charge the battery bank. This mode necessitates the bidirectional converter to act like a buck converter with a duty cycle of D_{b2}=0.22.

3. Design of System

Various operating stages of the developed system are properly designed to achieve the desired performance. The rating of SRM is 750 W with a rated speed of 1500 rpm. The peak output power of the solar panel is 860W, which is adequate to run the motor at its peak value. The design of different components of the developed system is given incoming sub-sections.

4.1. Solar Panel Selection

A solar panel with peak power point voltage and current (V_m, I_m) of 15.54 V and of 2.78 A, respectively, is chosen to get the essential power. First, the voltage of the solar panel at maximum power point is selected as $V_{mpp} = v_{pv}$ = 310 V. The other parameters are estimated as [16],

$$\text{The current at MPP, } I_{mpp} = i_{pv} = \frac{p_{pv}}{v_{pv}} = 860/310 = 2.78 \text{ A} \quad (1)$$

where $p_{pv} = P_{mpp}$ = 860 W is the output peak power. The modules linked in series are as,

$$N_s = \frac{V_{mpp}}{V_m} = 310/15.54 \approx 20 \quad (2)$$

And, the number of modules linked in parallel are as,

$$N_p = \frac{I_{mpp}}{I_m} = 2.78/3.08 = 1 \quad (3)$$

Connecting 20 modules in series, having 1 string in parallel, a PV array of required size is designed for this system.

4.2. Design of Bidirectional DC-DC Converter

Since, the bidirectional converter works in a boost or buck mode as per the necessity. So, the switches, S_{boost}, S_{buck}, are operated alternately. The magnitude of duty cycle D_{b1} under charge storage (bidirectional converter works in buck mode) is estimated as [15],

$$v_b = D_{b1} \times v_{dc} \Rightarrow D_{b1} = \frac{v_b}{v_{dc}} = \frac{240}{310} = 0.77 \quad (4)$$

Similarly, the value of the duty cycle when the battery is discharging the power to the SRM-pump (bidirectional converter works in boost mode) is estimated as,

$$v_{dc} = \frac{v_b}{(1 - D_{b2})} \Rightarrow D_{b2} = \frac{v_{dc} - v_b}{v_{dc}} = \frac{310 - 240}{310} = 0.22 \quad (5)$$

Therefore, the switching of the bidirectional converter is kept on varying between these values of duty cycles, D_{b1}, D_{b2} according to the working conditions.

According to these two values of duty cycles, there are two different sizes of an inductor, L_b corresponding to buck and boost mode operation. In buck mode of operation, S_{buck} is on and the energy is stored into the inductor, L_b. Similarly, when the bidirectional converter is in boost mode, S_{boost} is active and the inductor, L_b, discharges its stored energy. However, for both the modes, the value of the inductor is nearly the same. Therefore, the size of inductor L_b is estimated as,

$$L_b = \frac{D_{b1} \times v_b}{f_b \times \Delta i_b} = \frac{0.77 \times 240}{20000 \times 0.1 \times 28} \approx 3 \text{ mH} \quad (6)$$

4. Control Scheme

The control logic is designed for a developed system to operate efficiently under all working situations. The MPPT operation with battery management controls is achieved through a bidirectional converter. The BES control is dedicated to optimizing the charging/discharging performance of the battery bank and enables the flow of power in either direction. The other control is dedicated to the efficient motor drive operation. This motor control itself is divided into two sub-parts. The first part involves providing the soft-starting to the motor when back-emf is zero. Whereas, the second part of this control is responsible for the efficient steady-state operation of the drive and voltage balancing between two split DC link capacitors in steady-state and dynamic conditions. All these control techniques are elaborated in the following sub-sections.

5.1. Modified Solar Power Optimization

The conventional P&O MPPT approach is not much effective and has some limitations like deviation problems under varying insolation levels. The flow-chart of the conventional P&O MPPT technique is displayed in Fig.3. Thus, to overcome the limitations of the conventional approach, a modified P&O MPPT approach is implemented in the present system to strengthen the solar panel operation and improved its working under all situations [17]. The flow- chart of the executed MPPT

control is illustrated in Fig.4. This flow-chart is self-explanatory about the logics behind the implemented MPPT technique.

Fig.3. Logic of conventional MPPT scheme.

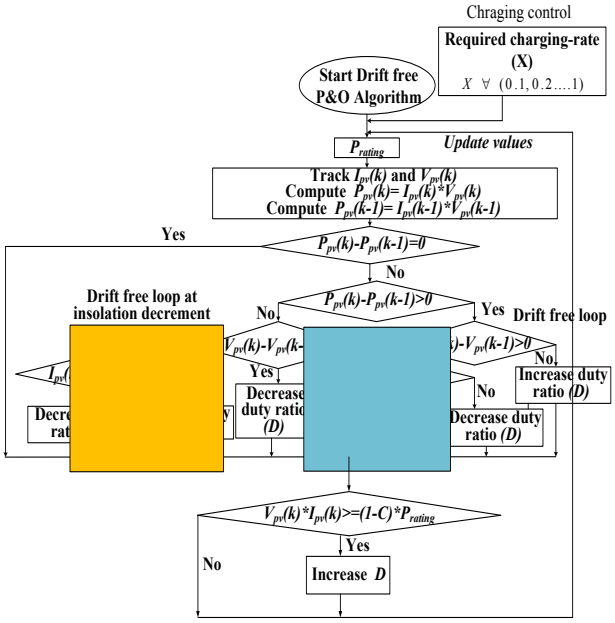

Fig.4. Logic for modified MPPT controller for solar power optimization

5.2. Voltage Balancing Approach With Drive Speed Control

The efficient operation of developed SRM drive at initial and in the steady-state situation, relies on mainly two control approaches. The first control technique ensures the soft-starting of a drive without using any current sensor at the motor side. Whereas, the second implemented control

at the motor side is responsible for the optimal selection of dwell angle for electronic commutation of SRM drive and to nullify the unevenness across split capacitors. Including various advantages, the utilized voltage balancing approach also offers a small switch and diode ratings SRM converter. The logic developed for the present drive is to work the system efficiently as well as to make voltage asymmetric compensation across two split capacitors under initial and in the steady-state situation, which is demonstrated in Fig. 4.

After measuring the voltages across both DC link capacitors, the compensation signal is provided to the commutation block. The comparison of the resultant duty cycle and a saw-tooth signal of 7 kHz frequency, results in PWM signals, 'S_1-S_4'. At final, both the signals, i.e. PWM pulses, 'S_1-S_4' and H1'-H4' signals including self-start control are merged with each other utilizing 'AND' logic. The final PWM switching scheme for a mid-point converter, 'T1-T4' is used to switch the mid-point converter.

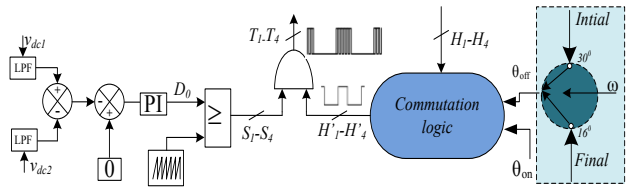

Fig.5. Motor control with voltage balancing for the SRM drive.

5.3. Control of Bidirectional Converter

The bidirectional battery controller used in conventional schemes [15-16] has limitations of uncontrolled charging/discharging of the battery and ineffective to the change in solar parameters dynamics. The structure of the basic conventional controller is shown in Fig.6. Thus, the present developed bidirectional controller has successfully acknowledged both these features and offers better performance of the overall system. The designed controller of the bidirectional converter is responsible for seamless power flow within the system by maintaining the desired voltage at the DC link. The main logic of the developed controller for the bidirectional converter is illustrated in Fig.7. This algorithm integrates the data of instantaneous PV array as well as a preset value of lower and upper battery current limits. In this correction, the overcharging or complete discharging of the battery is controlled by online estimation of the state of charge (SoC) of the battery by using its current and voltage magnitudes. There are various techniques available in the literature to estimate the SoC value online [18-19]. It is present in this method, if SoC is less than 20% then the discharge rate controller provides the zero signal to the switch, S_1 and the bidirectional converter stops working. On the other side, when SoC is more than 98% then the controller provides the zero signal to the switch, S_2 and there is no further charging, and the bidirectional converter becomes inactive. The maximum and minimum values of battery current are taken as 1.5A and 3.4A. The reference value of battery current is expressed as,

$$i_b = i_{b\_low.} + \frac{[(i_{b\_upp.} - i_{b\_low.}) \times v_{pv} i_{pv}]}{p_{pvpeak}} \qquad (7)$$

where, $i_{b\_upp.}$ and $i_{b\_low.}$ signify the preset limits. The term 'p_{pvpeak}' is the rated power of the solar panel.

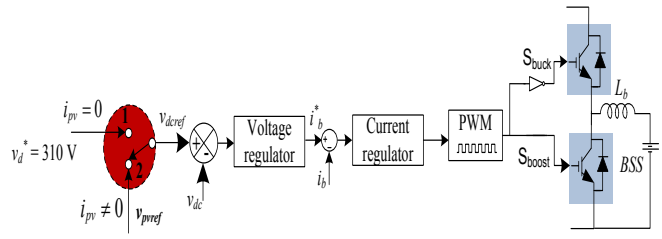

Fig.6. Logic for conventional bidirectional DC-DC converter controller.

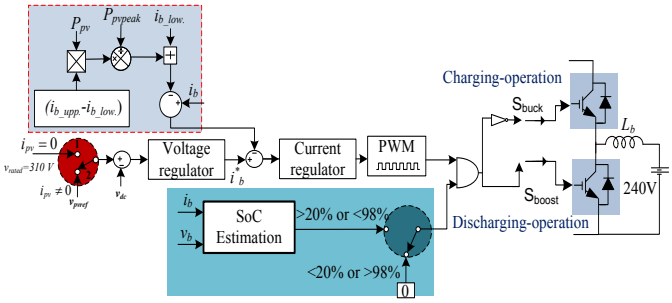

Fig.7. Modified Bidirectional converter controller.

Thus, the designed controller regulates the battery parameters within a set band regardless of the operating conditions. The BES terminal voltage variation at rapid insolation changes has been shown in Fig.8. It is observed that the scheme with a developed battery controller, has a better response of terminal voltage at insolation changes, which limits any high transient across BES, and it helps to improve the service life of the battery.

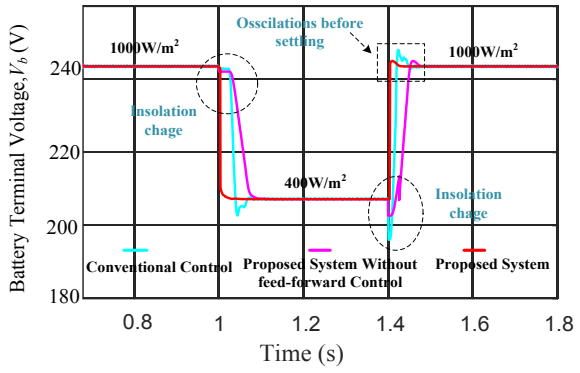

Fig.8. Battery terminal voltage performance for different systems.

5. *Simulated Performance*

The simulated performance of the developed scheme for solar water pumping is discussed and examined in detail in this part. The initial and steady-state performances are shown using simulated results in Figs. 9 to 12. The solar irradiances have changed from 1000W/m^2 to 500W/m^2 and then zero at 0.8s, and 0.95s, in order to determine the response of the system under continuously varying working conditions.

6.1 Starting and Steady-State Responses at Maximum Irradiance i.e. 1000W/m^2

Figs. 9 (a-b) illustrate the starting and steady-state performances of PV array (v_{pv}, i_{pv}, p_{pv}), battery (v_b, i_b) and SRM drive parameters (i_{ph1}, i_{ph2}, i_{ph3}, i_{ph4}, N, T_e and T_p) at STC, (1000W/m^2, 25^{0}C). In comparison to the double stage system, there is less ripple is observed in PV array parameters as illustrated in Fig. 9 (a). It is due to the removal of the DC-DC converter stage, which produces high switching ripples in the system. The smooth tracking of MPP voltage and generation of maximum output power i.e. 860 W from the PV array are displayed in Fig. 9 (a). The MPPT tracking duration is higher in this configuration due to the relatively large value of the PV array output capacitors. The positive value of battery current at starting to show it's discharging operation to provide the initial current to drive. After this, the battery current goes to zero similar to double-stage configuration, and the PV array provides the complete power to pump the water at installed capacity.

Moreover, the starting and steady-state performances of motor drive parameters, (i_{ph1}, i_{ph2}, i_{ph3}, i_{ph4}, N, T_e, and T_p) for this configuration are illustrated in Fig. 9 (b). Fig. 9 (b) depicts the starting and steady-state SRM drive parameters. The successful suppression of all four winding currents at starting and hence soft-starting of SRM are manifested in Fig. 9 (b). All the motor parameters are achieved their peak values and show the complete discharge of water at maximum insolation level with the battery in floating condition. The motor speed steadily rises to achieve the rated operating conditions. Thus, effective and proficient working is concluded by observing Figs. 9 (a-b).

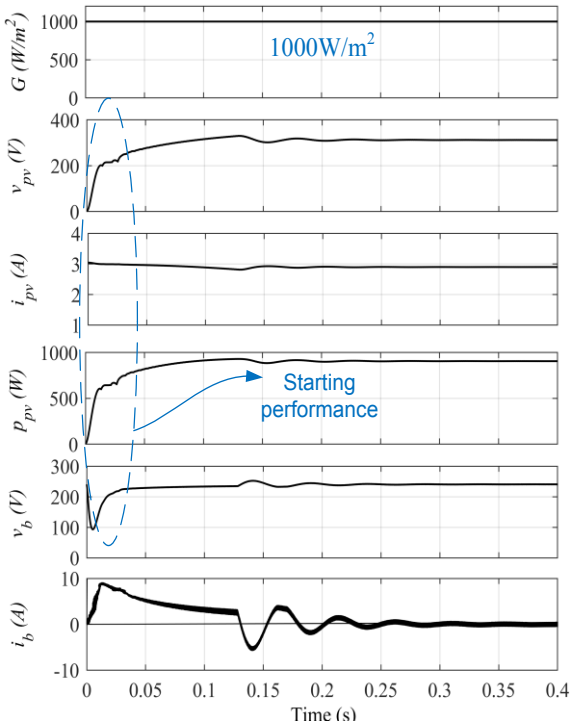

(a)

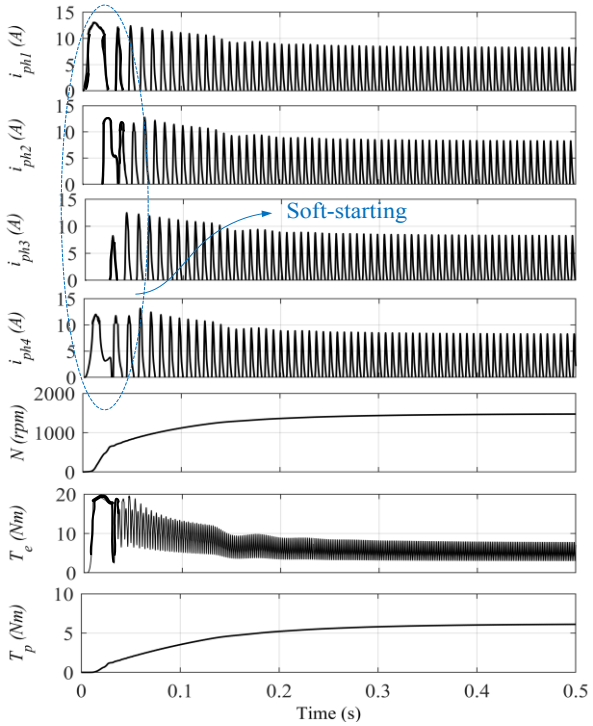

(b)

Fig. 9. Starting and steady-state performance at 1000W/m^2, (a) behavior of PV array and battery parameters, and (b) performance of SRM parameters.

6.2 Dynamic Behavior of System

The dynamic response of PV array (v_{pv}, i_{pv}, p_{pv}), battery (v_b, i_b) and SRM drive parameters (i_{ph1}, i_{ph2}, i_{ph3}, i_{ph4}, N, T_e and T_p) under varying insolation levels or absence of PV array power are demonstrated in Fig. 10. The performance of the system is tested under the same situation that has been for the double-stage configuration. It is observed from Fig. 10 (a) that the BES offers the extra power required to the SRM-pump under low irradiance conditions. However, the DC link voltage, v_{dc} is always maintained at the v_{pvref}. After 0.95s, when the solar power becomes zero, the battery discharges at its full value to alone provide the power to the SRM-pump. Although, the magnitude of v_{pvref} is zero, the DC link reference voltage is smoothly shifted to the fixed constant voltage, i.e. 310V as shown in Fig. 10 (a).

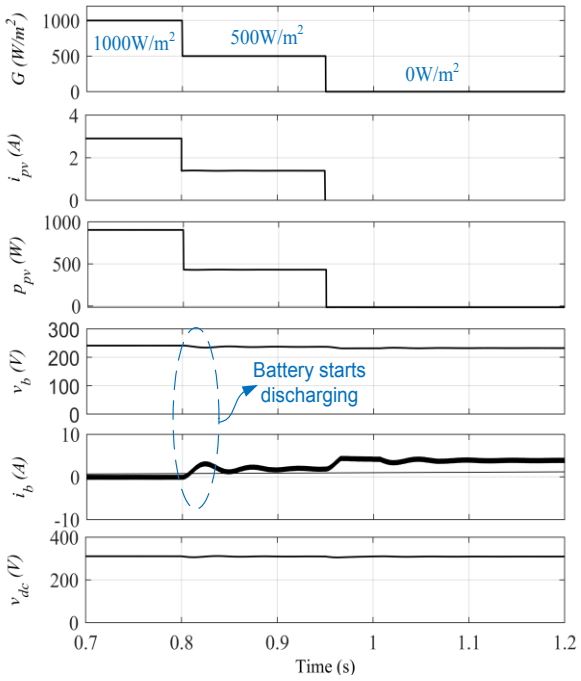

(a)

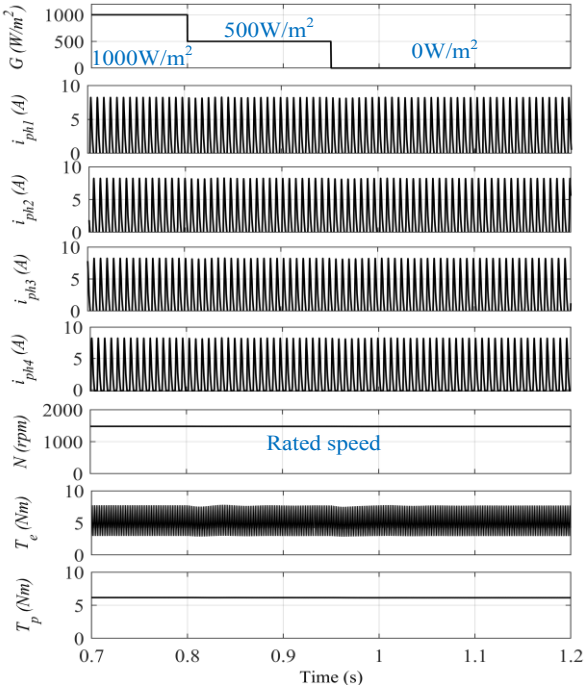

(b)

Fig. 10 Dynamic performance insolation change, (a) response of PV array and battery parameters, and (b) performance of SRM parameters.

The behavior of SRM parameters under this dynamic situation is also observed and exhibited in Fig. 10 (b). The uninterruptable operation of the SRM drive is governed by the constant speed and rated values of winding currents as illustrated in Fig. 10 (b). The speed of SRM is maintained at its rated value, i.e., 1500 rpm, and manifests the full volume of water also under dynamic

environmental conditions. Exactly similar to the double stage configuration, this configuration also has a satisfactory performance under dynamic conditions or even the absence of solar power.

6.3 Voltage Balancing Performance across DC-Link Split Capacitors under Dynamic Condition

Since, a certain DC link voltage is always present across the split DC link capacitors, it is also very critical and important to balance out the voltage across split capacitors. As the MPPT converter is not present, the voltage balancing together with the motor drive control is carried out using a mid-point converter. The starting and dynamic behaviors of v_{dc1}, v_{dc2} with and without the voltage balancing control are illustrated in Figs. 11 (a-b). The nature of v_{dc1}, v_{dc2} in starting, steady-state, and under dynamic conditions without implementing the voltage balancing control, is shown in Fig. 11 (a). In comparison to a two-stage system, the response is more severe. It is observed from Fig. 11 (a), that there is a huge difference between the two voltages and the motor would fail to start. There is also a difference in v_{dc1}, v_{dc2} under steady-state and under varying insolation changes, i.e. from 1000W/m^2 to 500W/m^2 and then 1000W/m^2, which leads to a ripple voltage of PV array and motor parameters. On the other side, there is a significant improvement in the performance of two voltages with the effect of voltage balancing control. The response of these two voltages with voltage balancing control is shown in Fig. 11 (b). Including the starting situation, the difference between the two voltages is also minimized in settled and in varying solar irradiance conditions as manifested by Fig. 11 (b).

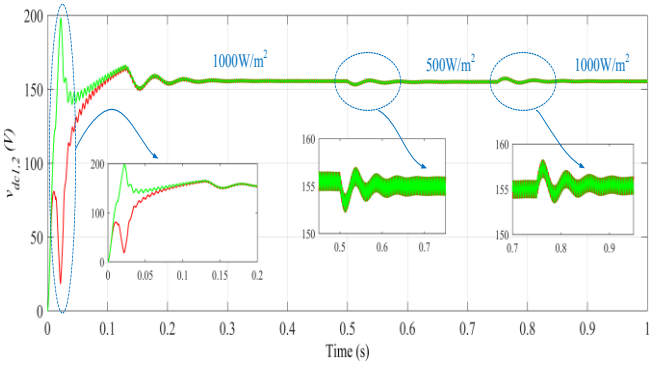

(a)

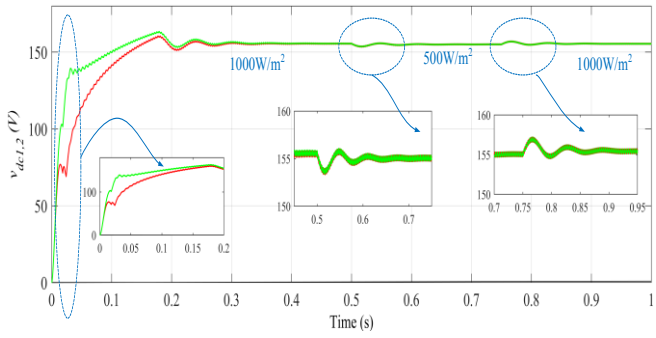

(b)

Fig.11 Response of voltage across DC-link split capacitors under varying irradiance, (a) without voltage balancing control, and (b) with voltage balancing control.

6.4 Performance at Sudden Start of Water Pumping

The performances of this system when the SRM drive is suddenly switched-on at the moment when the PV array power is generating its peak power and charges the battery at its full capacity, are shown in Figs. 12 (a-b). At the instant, when the motor operation is not needed, the battery side

converter is operated as a conventional buck converter. However, once the pumping is started, the same converter performs as a boost converter to achieve the MPP. The charging phenomenon of the battery is governed by the negative magnitude of i_b as illustrated in Fig. 12 (a).

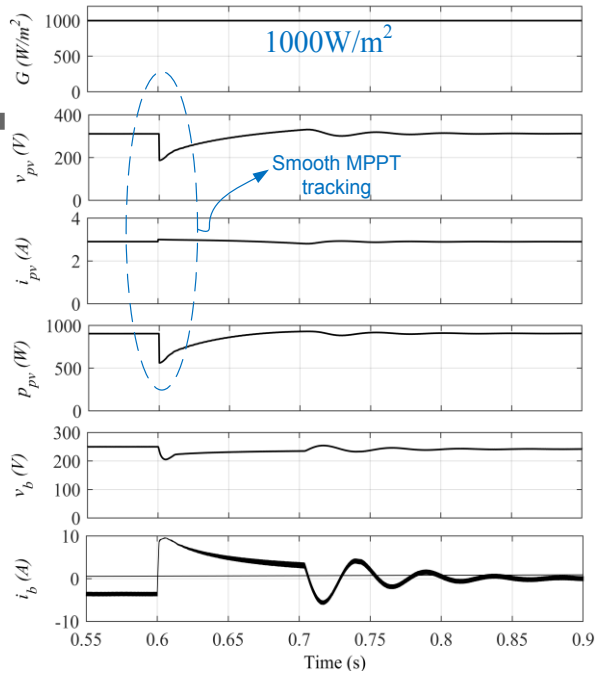

(a)

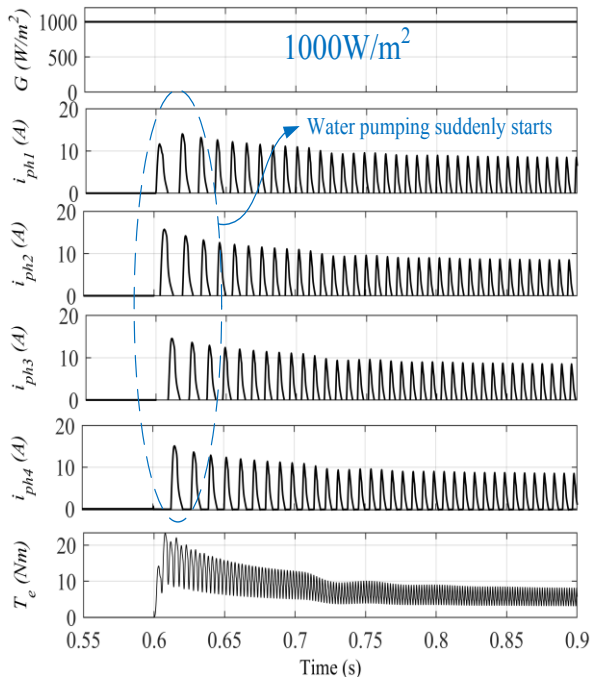

(b)

Fig. 12 Behavior of scheme while the water pumping is suddenly started under when PV array generates its peak power, (a) response of PV array and battery parameters and (b) performance of SRM parameters.

It is observed that the fluctuations in PV array and battery parameters are a little higher than the two-stage systems. However, all parameters are settled down within a few seconds and work normally. The behavior of SRM drive parameters under the situation, when it has suddenly started, is shown in Fig. 12 (b). All winding currents, i_{ph1}, i_{ph2}, i_{ph3}, i_{ph4} rise in a controlled fashion and manifest the successful soft-starting even under projected adverse conditions.

6. Experimental Results

The authentication of the developed WPS is carried out experimentally on a developed prototype in the laboratory. The setup includes a solar simulator, a mid-point converter, a battery pack, a bidirectional converter, and an SRM coupled to a DC generator. An AMTEK manufactured ETS600x17DPVF Terra SAS solar PV simulator is utilized to realize the solar PV array of 860W peak power capacity. A SEMIKRON make stack type number, MD B6U 415/560-50F+ MD B6C1 750/415-35F, converter is utilized to realize a bidirectional converter. Whereas, a SEMIKRON made stack type number, MD B6U 415/560-35F+ MD B2C1 600/415-30F, IGBT based converter is used as a mid-point converter in the developed experimental set-up.

The selection of battery specifications is done under some assumptions. It is considered that the PV power generation is for a maximum of 8 hours/day. Thus, the battery rating is selected such that the motor can operate minimum 7-8 hours short of utilizing PV power. For conceiving the needed capability of the battery stack, the terminal voltage, $v_{b,}$ and current, i_b are magnitude 240 V and 28 Ah. Hence, the developed system is able to operate the system at its full capacity even in the early morning, evening, or in night. Thus, a 240/28Ah SMF Exide battery bank with rack and enclosure is selected for the present system. The architecture of the developed signal conditioning board is demonstrated in Fig.13. To sense the voltage 'v_{pv}' and currents 'i_{pv}', 'i_b', Hall-Effect based voltage-current sensors (LV25P, LA55P) are employed, respectively. Additionally, the picture of the developed experimental set-up to validate the real-time effectiveness of the system is shown in Fig.14.

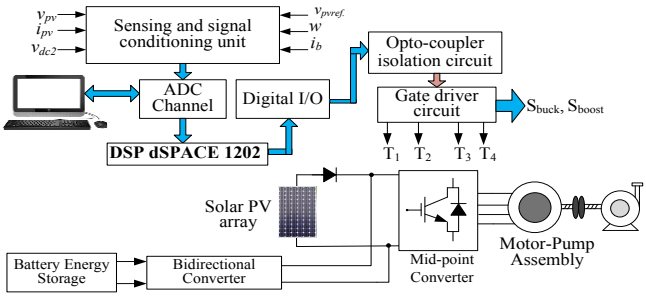

Fig.13 Control architecture of the developed system.

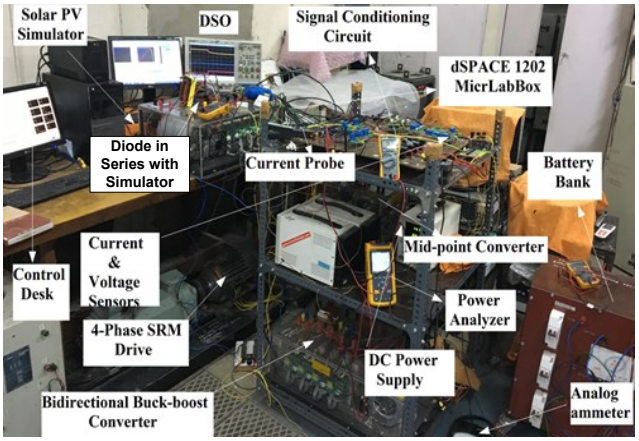

Fig.14 picture of the developed experimental setup.

7.1 Behavior of System Indices when Solar PV Panel Alone Runs Pump

The nature of v_b, i_b, and motor parameters in mode I, is demonstrated using Figs. 15 (a-d). The responses of v_b, i_b, winding current of SERM, i_{ph1} are illustrated in Fig. 15 (a). The captured results demonstrate the skilled soft-starting and perfect MPPT operation in steady-state conditions. It also shows that the motor speed is achieved its peak magnitude and so the system is able to supply the full volume of water under this working condition. The battery connected to the system is in an idle situation and assists to maintain the MPPT operation without any power exchange.

Whereas, Fig.15 (b) presents the response of motor parameters, i_{ph1}, v_{ph1}, i_n at 1000W/m^2 under settled condition. It is worth mentioning that the phase voltage is nearly half of the rated DC-Link voltage and, therefore, the required rating of the IGBT switch for the SRM converter is also small as compared to other similar motor-driven converters. The dynamic performance of system parameters especially, solar panel and motor side is shown in Fig.15(c). It is seen that in this mode I, the MPPT controller is acting very effectively and optimized the solar performance through the bidirectional converter control. Since, the reference, DC link voltage is the same as the MPPT voltage and, therefore, the same magnitude equal to 'v_{pv}', is appeared across the DC link voltage. The response of the implemented MPPT controller is displayed in Fig.15 (d). It is remarked that the tracking efficiency is more than 99% and governs the successful optimization of solar power. Moreover, the generated power is 860 W, which signifies a considerable reduction in losses due to a reduction in intermediate DC-DC MPPT converter.

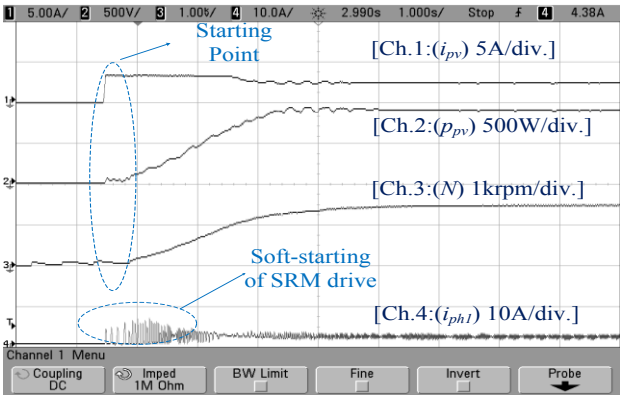

(a)

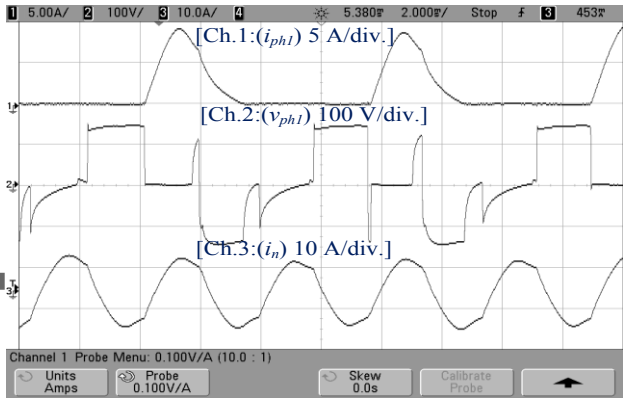

(b)

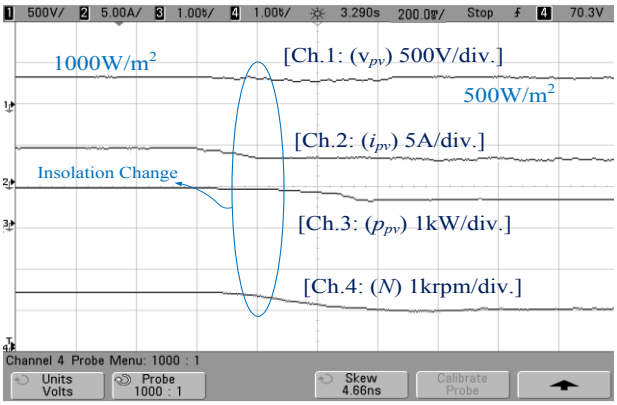

(c)

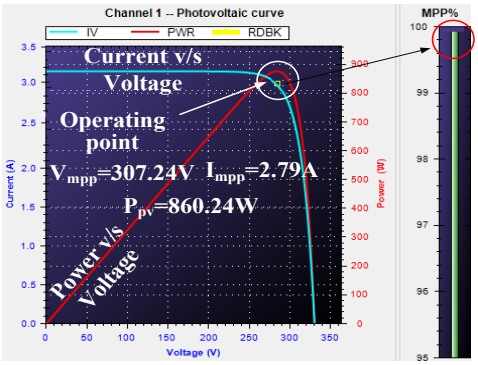

(d)

Fig. 15. Performance of system parameters, (a) behavior of i_{pv}, p_{pv}, i_{ph1}, N in starting condition (b) steady-state performance of i_{ph1}, v_{ph1}, i_n, (c) dynamic performance under irradiance variation and (d) % MPPT performance under 1000W/m^2 irradiance.

7.2 Battery Alone Runs Pump

The nature of v_b, i_b, and motor parameters mode II, is demonstrated in Figs. 16 (a-b). The responses of indices i_{ph1}, N, v_b, i_b in both starting as well as in settled conditions are given in Fig.16 (a). The controlled rising of motor phase current and battery discharging current manifest the efficacy of developed control techniques. The positive value of battery current and a sharp decrease in battery terminal voltage show the discharging of battery stored energy. On the other side, the perfect voltage balancing through the SRM converter is shown in Fig.16 (b). Both the magnitudes of v_{dc1}, v_{dc2}

are perfectly equal and balanced throughout the operation. The PWM switching operation of the motor converter is observed by the nature of winding current, i_{ph1}.

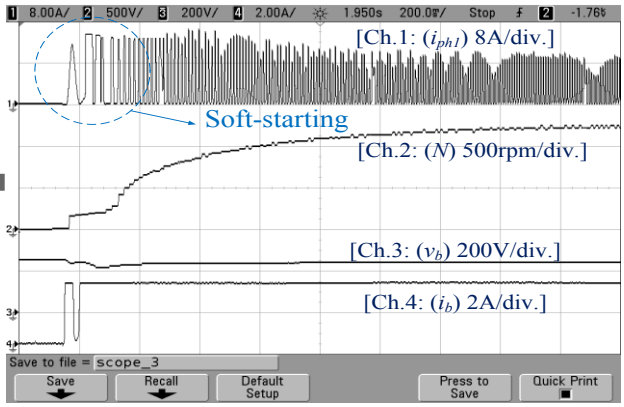

(a)

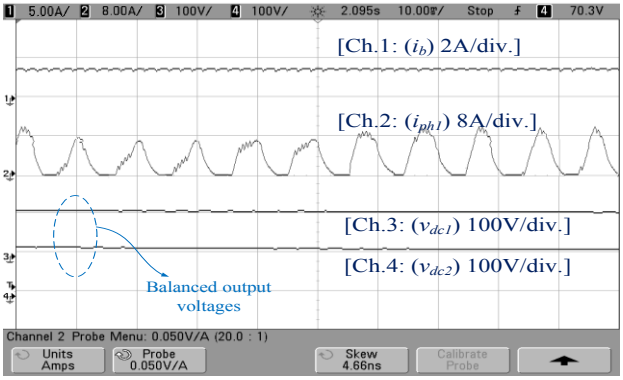

(b)

Fig. 16. The system behavior when only battery drives the motor, (a) Starting response of i_{ph1}, N, v_b, i_b, and (b) steady-state response of i_b, i_{ph1}, v_{dc1}, v_{dc2}.

7.3 Dynamic Performance at Varying Insolation Levels

The behaviors of v_{pv}, v_b, i_{pv} and i_b under irradiance variation i.e. from 800 W/m^2 to 400 W/m^2 are illustrated in Fig.17 (a). It is observed that there is a momentary dip in solar output voltage, v_{pv} under the change in insolation levels from 800W/m^2 to 400W/m^2. However, within a fraction of a second, it again attains its MPP value and operates efficiently at lower insolation level. The increase in the magnitude of battery current governs the smooth supply of required power by the storage battery to the drive for the uninterrupted full volume of water pumping. Fig. 17 (b) shows the condition when there is an increase in insolation from 500W/m^2 to 1000W/m^2 in mode II when PV panel power is not adequate to run the pump at its full rating. As it is demonstrated by Fig. 17 (b), the speed of the drive is unaffected by this insolation change and runs at its full speed.

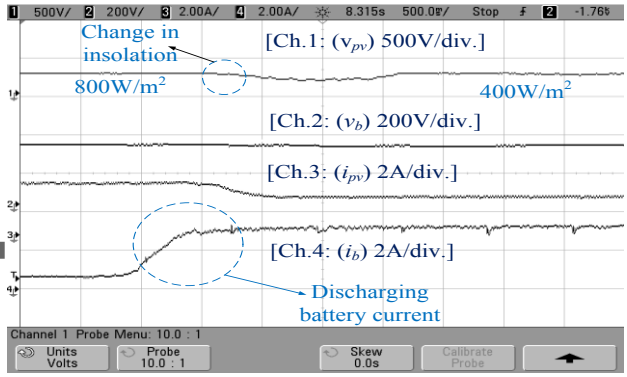

(a)

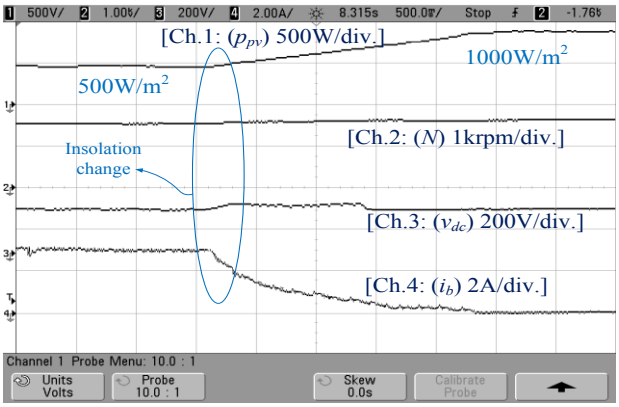

(b)

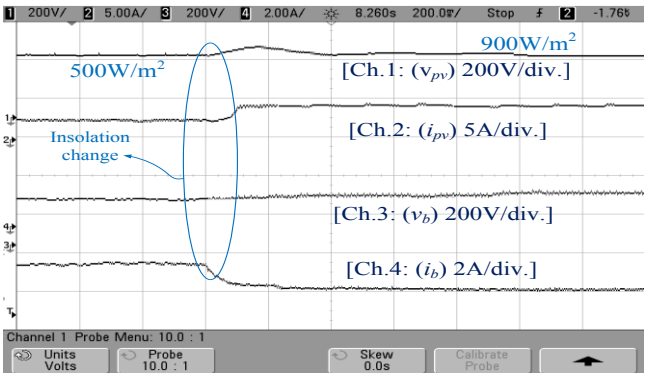

(c)

Fig.17. Dynamic performances, (a) v_{pv}, v_b, i_{pv}, i_b in mode II with a decrease in insolation, (b) p_{pv}, N, v_{dc}, i_b in mode II with an increase in insolation, and (c) v_{pv}, v_b, i_{pv}, i_b in mode IV.

There is also a successfully maximum power tracking in this mode. Moreover, the effectiveness of the implemented MPPT approach and the achievement of desired performance of the system in mode IV are illustrated in Fig.17(c). In this case, when water output is not obligatory, and the battery stack is getting charged through available PV array power.

7.4 When Solar PV Array Power is Suddenly Out and Pump is Running with Battery

One more probable condition is usually encountered in the rainy seasons when the system is operating at its full capacity and suddenly output of solar PV array becomes zero. The behavior of system parameters v_{pv}, i_{ph1}, $v_{dc,}$ and i_b under such conditions, is demonstrated in Fig. 18. There is a small drop in PV array voltage i.e., 'v_{dc}' is observed at the moment when solar power has gone. However, v_{dc} is again maintained its reference value, i.e., 310V. The positive magnitude of current, i_b in Fig. 18, demonstrates the full discharge of the battery bank to run the system at its rated value.

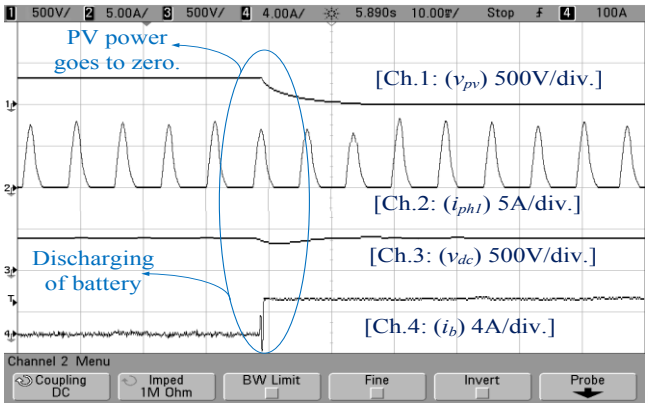

Fig.18. Behavior of p_{vp}, i_{ph1}, $v_{dc,}$ and i_b when PV array power is suddenly gone, and battery alone runs the SRM-pump arrangement.

7.5 The behavior of Developed System when Pump is Abruptly Closed

This section represents the behavior of system parameters when suddenly the pump is switched off and the available solar power is diverted from the drive to the battery storage. The disappearance of the motor winding current in the middle of the operation signifies the removal of the load.

Table 1. Comparative Analysis Between Existing and Present System

Configurations	Motor Converter topology	Control Scheme	Benefits	Major Shortcomings
Conventional [10]	(n+1) converter topology (Miller converter)	Hysteresis control	• Uninterrupted water supply • Solar output capacitor not required	• Higher switching losses • Overvoltage damper failure • Inefficient MPPT controller • Uncontrolled charging/discharging of the battery pack • No real-time validation
Conventional [15]	Split DC-link converter	Single pulse mode	• Uninterrupted water supply • Low motor converter losses	• Requirement of MPPT DC-DC converter • Inefficient MPPT controller • Uncontrolled charging/discharging of the battery pack • Slow dynamic response • High ripples in battery charging current
Conventional [16]	Split DC-link converter	Single pulse mode	• Uninterrupted water supply • Low motor converter losses • Absence of MPPT DC-DC converter	• Inefficient MPPT controller • Uncontrolled charging/discharging of the battery pack • System not tested for all modes • No PV panel performance optimization provision under mode IV

Present Scheme	Split DC-link converter	Single pulse mode	• Uninterrupted water supply • Low motor converter losses • Absence of MPPT DC-DC converter • Controlled charging/discharging of the battery pack • Effective MPPT controller • Solar power optimization in all possible modes	• Higher motor converter losses in mode II due to high-frequency switching

The performance of various parameters of the system is shown in Fig.19. In this case, there is fluctuation in DC link voltage, but it is settled down within a small span of time. The battery is now receiving solar power and charges to its maximum capacity. Moreover, a comparison between conventional systems [10], [15-16] and proposed topology considering various aspects has also been done and given in Table 1. It is seen that the present scheme is successfully overcomes all the limitations of the existing system and has various benefits over them.

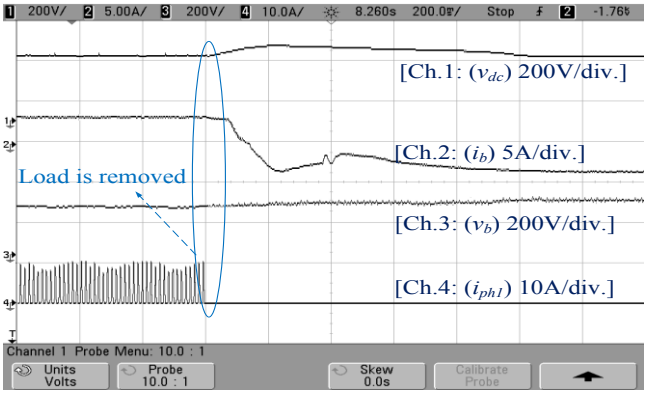

Fig. 19. Behavior of v_{dc}, i_b, v_b, i_{ph1} when the pump is suddenly switched-off in mode II.

8 CONCLUSION

A battery supported solar PV array-water pumping system with an SRM drive has been used, and their applicability has been exhibited using a MATLAB/Simulink platform. Additionally, the responses achieved via simulation have been verified on an experimental setup. The battery support acts as a secondary energy source linked at the common DC link in present configurations. An efficient power streaming control scheme has been developed and implemented in the present scheme. The developed voltage balancing technique to maintain the equal voltage across DC-link split capacitors has been observed to perform perfectly. Besides, the design logic has enabled uninterrupted water pumping with the full volume of water delivery, irrespective of the climatic conditions. Overall, this topology has emerged as a reliable and efficient water pumping system.

9 REFERENCES

[1] M. Al-Soeidat, T. Cheng, D. D. Lu, and V. G. Agelidis, "Experimental study of static and dynamic behaviors of cracked PV panels," *IET Rene. Power Generation*, vol. 13, no. 16, pp. 3002-3008, 9 12 2019.

[2] M. Emmanuel, J. Giraldez, P. Gotseff, and A. Hoke, "Estimation of solar photovoltaic energy curtailment due to volt–watt control," *IET Renewable Power Generation*, vol. 14, no. 4, pp. 640-646, 16 3 2020.

[3] R. Subramanian, C. Murugesan, S. Tamilkolundu, and D. Jaganath, "Enhancement of wind speed using converging duct for cooling off-grid mast-mounted flat solar PV panels to improve its power generation," *IET Renewable Power Generation*, vol. 14, no. 2, pp. 263-269, 3 2 2020.
[4] S. Murshid and B. Singh, "Energy-efficient single-stage solar PV powered sensorless PMSM drive for water pumping," *IET Renewable Power Generation*, vol. 13, no. 13, pp. 2267-2277, 7 10 2019.
[5] N. Priyadarshi, M. S. Bhaskar, S. Padmanaban, F. Blaabjerg, and F. Azam, "New CUK–SEPIC converter based photovoltaic power system with hybrid GSA–PSO algorithm employing MPPT for water pumping applications," *IET Power Electronics*, vol. 13, no. 13, pp. 2824-2830, 14 10 2020.
[6] J. Meyer and S. von Solms, "Solar Powered Water Security: An Enabler for Rural Development in Limpopo South Africa," *IEEE Access*, vol. 6, pp. 20694-20703, 2018.
[7] O. S. Ebrahim, M. A. Badr, A. S. Elgendy and P. K. Jain, "ANN-Based Optimal Energy Control of Induction Motor Drive in Pumping Applications," *IEEE Transactions on Energy Conversion*, vol. 25, no. 3, pp. 652-660, Sept. 2010.
[8] A. Kumar Mishra and B. Singh, "Efficient solar-powered water pump with single-input dual-output DC-DC converter employing four-phase SRM drive," *IET Power Electronics*, vol. 13, no. 15, pp. 3435-3444, 25 11 2020.
[9] K. R. Dhumal and S. S. Dhamse, "Solar PV Array-Based Water Pumping by Using Srm Drive: A Review," in *Proc. International Conference on Computation of Power, Energy, Infor. and Communication (ICCPEIC)*, Chennai, 2018, pp. 140-146.
[10] X. Wang, C. Gan, Y. Hu, W. Cao, and X. Chen, "Renewable energy-fed switched reluctance motor for PV pump applications," in *Proc. IEEE Conference and Expo Transportation Electrification Asia-Pacific (ITEC Asia-Pacific)*, Beijing, 2014, pp. 1-6.
[11] A. Khare and S. Rangnekar, "Optimal sizing of a grid integrated solar photovoltaic system," *IET Renewable Power Generation*, vol. 8, no. 1, pp. 67-75, January 2014.
[12] J. Wang and F. Yang, "Optimal capacity allocation of standalone wind/solar/battery hybrid power system based on improved particle swarm optimization algorithm," *IET Rene. Power Generation*, vol. 7, no. 5, pp. 443-448, Sept. 2013.
[13] M. Khalid, M. AlMuhaini, R. P. Aguilera and A. V. Savkin, "Method for planning a wind-solar–battery hybrid power plant with optimal generation-demand matching," *IET Renewable Power Generation*, vol. 12, no. 15, pp. 1800-1806, 19 11 2018.
[14] R. Hollinger, L. M. Diazgranados, F. Braam, T. Erge, G. Bopp and B. Engel, "Distributed solar battery systems providing primary control reserve," *IET Renewable Power Generation*, vol. 10, no. 1, pp. 63-70, 1 2016.
[15] V. Narayana, A. K. Mishra, and B. Singh, "Design of SRM driven BESS based PV powered water pumping system," in Proc. IEEE 7th Power India Intel. Conference (PIICON), Bikaner, 2016, pp. 1-6.
[16] A. K. Mishra and B. Singh, "Stage Solar PV Powered Water Pump with a Storage System," in *proc. 8th IEEE India International Conf. on Power Electronics* (IICPE), JAIPUR, India, 2018, pp. 1-6.
[17] J. Mishra, M. Pattnaik and S. Samanta, "Drift-Free Perturb and Observe MPPT Algorithm With Improved Performance for SEIG-Based Stand-Alone Wind Energy Generation System," *IEEE Transactions on Power Electronics*, vol. 35, no. 6, pp. 5842-5849, June 2020.
[18] Z. Xia and J. Abu Qahouq, "State-of-charge Balancing of Lithium-ion Batteries with State-of-health Awareness Capability," *IEEE Transactions on Industry Applications*. (Early Access)
[19] R. Rudnik, C. Wang, L. Reyes-Chamorro, J. Achara, J. -Y. L. Boudec and M. Paolone, "Real-Time Control of an Electric Vehicle Charging Station While Tracking an Aggregated Power Setpoint," *IEEE Transactions on Industry Applications*, vol. 56, no. 5, pp. 5750-5761, Sept.-Oct. 2020.

Appendices

Hardware parameters: P_{rated} = 1 hp, 4 phase, 157 rad/s, unaligned and aligned inductances, L_u=10mH, L_a= 110mH. Solar module: V_{oc} = 350 V, I_{sc} = 3.5 A, SMF Exide battery bank indices: V_b= 240 V, Ah = 28 Ah, L_b= 2mH, $C_{DC,12}$ = 500 µF, bidirectional converter controller: K_p = 0.12, Ki = 0.08, current controller: K_p = 0.21, K_i = 0.82, sampling time = 40 µs.